Journal of Microwaves, Optoelectronics and Electromagnetic Applications, Vol. 24, No. 3, e2025290613 Sep 2025
DOI: http://dx.doi.org/10.1590/2179-10742025v24i3290613

Uplink Performance under High Traffic Demand in Massive LoRaWAN

Fernando S. Sousa[1], Ivan R. S. Casella[1], Carlos E. Capovilla[1]
[1]*Federal University of ABC, Santo Andre, SP, Brazil,*
f.simplicio@ufabc.edu.br, ivan.casella@ufabc.edu.br, carlos.capovilla@ufabc.edu.br

***Abstract*– LoRaWAN (Long Range Wide Area Network) is an innovative and mature solution for IoT (Internet of Things) applications. It allows network devices to transmit their data whenever necessary, without the need for any coordination or scheduling mechanism, by employing the multichannel P-ALOHA (Pure-ALOHA) random access protocol. However, in massive LoRaWAN scenarios, transmissions on the same channel often result in collisions, significantly reducing throughput and quality of service. In this context, this work aims to analyze the performance of the uplink of a massive LoRaWAN through computational simulations for different operation conditions and propagation scenarios. To obtain more realistic and representative results, signal propagation losses are estimated by combining the COST231-Walfisch-Ikegami (COST231-WI) model with the TMM (Terrain Modeling Module), the DEM (Digital Elevation Model) and the DTED (Digital Terrain Elevation Data) of the OPNET Modeler simulation platform. The results obtained in the analyses carried out highlight the challenges imposed on the LoRaWAN in terms of scalability and energy efficiency, especially in environments with high device density.**

***Index Terms*–** COST231, IoT, LoRa, LoRaWAN, P-ALOHA.

I. Introduction

LoRaWAN (Long Range Wide Area Network) is an innovative solution developed for low rate applications that has emerged as one of the most promising wireless network technologies for IoT (Internet of Things) [1], [2]. As its PHY (Physical) layer is based on LoRa (Long Range) technology, it operates in the license-free ISM (Industrial, Scientific and Medical) frequency bands and features good robustness to interference, high energy efficiency and wide coverage [3].

Despite its advantages, the scalability of LoRaWAN is limited by the use of the multichannel P-ALOHA (Pure-ALOHA) random access protocol, which lacks packet transmission control mechanisms [4], [5]. Since in this protocol devices can transmit packets at any time without scheduling, collisions and packet losses will occur, causing rapid performance degradation as the number of devices and network load increase [6]–[9]. Furthermore, terrain characteristics as well as the presence of obstructions (e.g. buildings) can cause significant variations in the received signal, which can affect the range and performance of the network [2].

To address the aforementioned challenges, this article presents an in-depth analysis of the performance impact of using the multichannel P-ALOHA protocol on the uplink of a LoRaWAN in massive scenarios (i.e. with high device density). For this, several performance metrics are considered, such as throughput, error rate, collision rate, successful received packet rate, delay, and energy consumption. To ensure more realistic and representative results, signal propagation losses are estimated by integrating the COST-231

Walfisch-Ikegami (COST231-WI) model with the TMM (Terrain Modeling Module), the DEM (Digital Elevation Model) and the DTED (Digital Terrain Elevation Data) of the OPNET Modeler simulation platform. This integration is essential to automatically take into account the relief characteristics and obstacles within the coverage area in the different massive scenarios analyzed and to improve the accuracy of the results.

In addition to this introductory section, this article is composed of the following sections: Section II reviews some articles related to this work. Section III provides an overview of the LoRaWAN architecture. Section IV describes the modeling developed for the uplink of the massive LoRaWAN under study. Section V presents the results of the analyses performed. Section VI shows a deeper assessment of the energy waste on the LoRaWAN uplink. Finally, the main conclusions are presented in Section VII.

II. Related Works

Given the increasing use of LoRaWANs in different IoT applications, it becomes essential to analyze their performance in more depth (e.g. throughput, delay, energy consumption), which strongly depends on the intrinsic characteristics of the LoRa technology (e.g. modulation type, duty cycle) and on regulatory aspects that provide guidelines and usage restrictions [10]. In the following, some relevant works that address these issues using the OPNET Modeler (or equivalently, the Riverbed Modeler) are present [11].

In [12], the authors propose a simulation environment for LoRa systems in the OPNET Modeler. The paper begins by detailing the characteristics of the LoRa PHY layer and MAC (Medium Access Control) sublayer, as defined by the LoRa Alliance specifications (i.e. single frequency channel). Then, the developed simulation environment is described, emphasizing the implementation of the PHY layer, which incorporates the relationship between the bit error rate BER and the bit energy-to-noise power density ratio E_b/N_0 of LoRa systems. Furthermore, the article briefly describes how to develop the ED (End Device), GW (Gateway), and NS (Network Server) models using the OPNET Modeler hierarchical structure.

In [13], the authors developed a LoRaWAN simulation environment using the Riverbed Modeler to investigate the impacts of packet collisions and interference in the coverage and throughput of LoRaWANs. In addition to using the Hata rural path loss model, this work incorporates features such as the relationship between BER and spreading factor SF, and the limits of signal-to-interference plus noise ratio $SINR_{dB}$ for inter-SF and intra-SF interference. Three collision models are evaluated: a pessimistic baseline model where simultaneous transmissions result in packet losses, a capture-effect model allowing the reception of packets with the highest $SINR_{dB}$ for each SF, and a more complex inter-SF interference model. The simulations were conducted for a LoRaWAN with P-ALOHA in two perspectives: one with EDs using $SF7$ fixed at distances of 10-50 km from the GW and another with EDs randomly assigning $SF7$ to $SF12$ in a circular area with a radius of 13 km, centered on the GW. The results indicate throughput differences ranging from 7.1% to 100.1% for $SF7$, while for multiple SFs, the differences extended to 18.4% to 323.7% for intra-SF interference and 15.3% to 240.3% for inter-SF interference. This highlights the negative impact of strictly periodic traffic combined with the duty cycle limitations of LoRaWAN on channel utilization.

Similarly, LoRaWAN performance has also been investigated in [14], where the authors relied on the LoRaWAN models presented by [15] and the analyses of [13] to meet the demands of future IoT

Brazilian Microwave and Optoelectronics Society-SBMO received 25 Sep 2024; for review 15 OCt 2024; accepted 06 Apr 2025
Brazilian Society of Electromagnetism-SBMag ISSN 2179-1074

applications and support mMTC (massive Machine-Type Communications) in next-generation wireless systems beyond 5G (Fifth Generation). A single frequency channel was used in the simulations and packet delivery ratio and throughput were estimated. As a result, it was observed that as the number of active devices increases dramatically, interference will become a significant limiting factor.

III. LoRaWAN Architecture

LoRaWAN is an open wireless networking standard with star topology that offers long range, low power consumption, enhanced security, and flexibility through a centralized architecture for the configuration, monitoring and control of connected devices [16]. The main elements of a LoRaWAN are: EDs, GWs and the NS, each playing distinct roles in the different layers of the network [17].

EDs are responsible for transmitting and receiving data over the network. They can operate in Class A mode, the most energy-efficient mode, where an uplink message is first transmitted and then two short reception windows are opened to receive possible downlink messages from the NS (typically via a GW). Outside these intervals, EDs remain in low power mode, making Class A operation ideal for applications that require minimal power consumption [18]. The MAC sublayer of the EDs uses the P-ALOHA multiple access technique which, although energy efficient, is prone to packet collisions, especially in massive LoRaWANs. These collisions reduce the data throughput and overall network performance [16].

GWs act as intermediate nodes between EDs and the NS. Typically equipped with multichannel transceivers, GWs can receive transmissions from multiple EDs simultaneously [19]. Once the GWs receive packets, they forward them to the NS via TCP (Transmission Control Protocol) [17].

The NS is responsible for authenticating and validating received packets, ensuring data integrity and security [17]. The NS also routes packets to their destinations, coordinating communication between EDs and network applications. Through these centralized network control and management functions, the NS ensures efficient, continuous and secure operations within the LoRaWAN.

The LoRaWAN PHY layer is built on top of the LoRa specifications, which designate CSS (Chirp Spread Spectrum) as its main modulation technique. In CSS, frequency chirps are employed to increase the robustness of the communication link against interference and multipath fading [7]. The relationship between the transmitted data rate and the bandwidth BW is determined by the SF. The higher the SF, the lower the data rate but the greater the range. In this way, the data rate can be adjusted to optimize the performance of the LoRaWAN as a function of the distance d and the transmission power $P_{t_{dBm}}$ of each network device [6]. Thanks to the orthogonality between different CSS signals, devices can transmit simultaneously without causing interference to each other, employing different values of SF where, according to the LoRa specifications, $SF \in \{7, ..., 12\}$ [20].

In addition to CSS, LoRa also employs FCH (Frequency Channel Hopping) and FEC (Forward Error Correction) techniques to further improve the robustness and range of communication links. In LoRa FCH, the uplink frequency channels are pseudorandomly selected over time to reduce the probability of collisions [19]. On the other hand, the LoRa FEC scheme is based on Hamming coding and the desired error correction capability can be adjusted by the code rate CR. However, increasing CR causes a higher bit overhead and a reduction in the effective bit rate R_b [7], [21], [22]. The relationship between R_b, SF, CR and the symbol period T_s is presented in (1):

$$R_b = \frac{SF}{T_s} \cdot CR \tag{1}$$

  ISSN 2179-1074

where $T_s = \frac{2^{SF}}{BW}$ and $CR = \frac{4}{4+cr}$ for $cr \in \{1, 2, 3, 4\}$, indicating the number of error-correcting bits added to the transmitted data.

IV. Massive LoRaWAN Model Description

The PHY layer and MAC sublayer of the uplink of the analyzed LoRaWAN are developed using three distinct levels of the hierarchical structure of the OPNET Modeler. At the highest level, the network domain defines the global structure of the network, describing the star topology of the modeled system. It uses the Earth's global coordinate system to precisely locate the EDs, ensuring accurate representation of the network's geographical layout. The next level, the node domain, specifies node models that represent the structure of the objects within the modeled system, such as EDs, GWs and the NS. These node models include predefined modules that reference process models, such as transmitters and receivers. Lastly, at the lowest level, the process domain defines models that describe the system's behavior. These process models are created using state and transition diagrams, complemented by Proto-C based object-oriented programming [11].

A. OPNET Network Domain

In the OPNET network domain, two different scenarios are developed to evaluate the uplink performance of the analyzed LoRaWAN under different operating conditions. In Scenario-1, the modeling of the communication channels takes into account the effect of the AWGN (Additive White Gaussian Noise), while in Scenario-2, the effect of the multipath fading is also considered, in addition to AWGN.

In the analyses of both scenarios, the predominantly flat suburban region composed of houses shown in Fig. 1 is used. The region is delimited by a circle with a radius of 750 meters around a central GW, positioned at latitude -22.871085 and longitude -47.206232, and divided into 6 sub-regions equally spaced by 125 meters. The total number of EDs N_{ED} is fixed as 600 and the EDs are organized into 6 groups of 100, each operating in Class A mode with a different SF (values increasing from 7 to 12 from the central GW) and randomly distributed within each sub-region.

The radius of the region, as well as the distance limits of each sub-region, are defined based on the performance achieved by each SFs in field tests [23]. It is considered that the EDs operate with a $P_{t_{dBm}}$ of 20 dBm, a BW of 125 kHz and a CR of $\frac{4}{5}$. Each ED is equipped with an isotropic antenna mounted at a height of 2 meters above the ground, transmitting packets with a fixed size of 46 bytes. The GW also uses an isotropic antenna, but positioned at a height of 6 meters above the ground.

The OPNET Modeler DEM functionality is employed to integrate the DTED into the simulation environment. This digital data set is given by the matrix of terrain elevation values from the region under study. During the field measurements, development kits with LoRa SX1276 modules [24] were used, allowing the measurement of the received power $P_{r_{dBm}}$ for each SF at different distances [23].

COST231-WI is a semi-deterministic model designed to estimate path loss in the 800 MHz to 2 GHz band, for both LOS (Line-of-Sight) and NLOS (Non-Line-of-Sight) conditions [25]. For the LOS condition, the COST231-WI path loss in dB can be estimated by (2):

$$L_{\mathrm{LOS}_{dB}} = 42.6 + 26 \cdot \log_{10}(d) + 20 \cdot \log_{10}(f_c) \tag{2}$$

where f_c is the signal frequency in MHz and d is the distance between the GW and the ED in km.

  ISSN 2179-1074

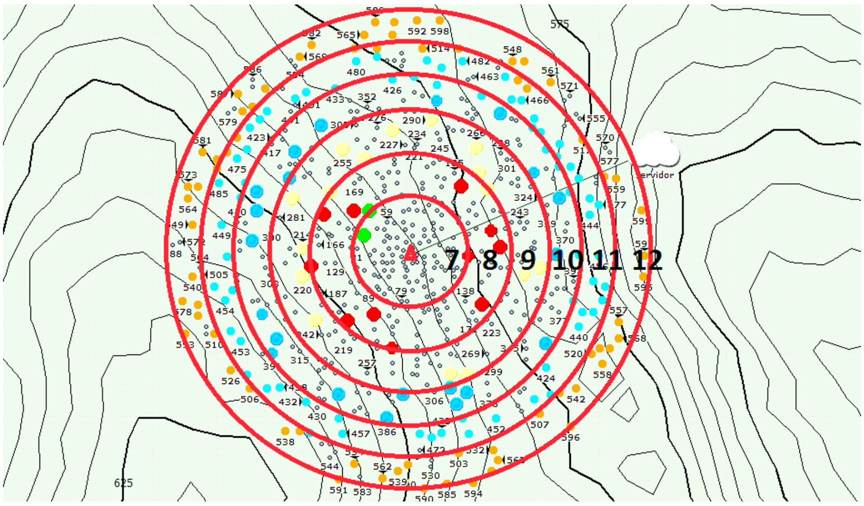

Fig. 1. LoRaWAN scenario featuring EDs grouped by SF with a central GW. Each group consists of 100 EDs, where $SF7$ devices are positioned closest to the GW, and $SF12$ devices are placed farthest from it.

For the NLOS condition, the path loss combines three main components: free-space loss L_0, diffraction and scattering loss from rooftop to street L_{rts} and multi-screen diffraction loss L_{ms}, and can be represented in dB by (3):

$$L_{\text{NLOS}_{dB}} = \begin{cases} L_0 + L_{rts} + L_{ms}, & L_{rts} + L_{ms} \geq 0 \\ L_0, & L_{rts} + L_{ms} < 0 \end{cases} \tag{3}$$

The term L_0 in (3) is given by (4):

$$L_0 = 32.45 + 20 \cdot \log_{10}(d) + 20 \cdot \log_{10}(f_c) \tag{4}$$

On the other hand, the term L_{rts} in (3) is represented by (5):

$$L_{rts} = -16.9 - 10 \cdot \log_{10}(w) + 10 \cdot \log_{10}(f_c) + 20 \cdot \log_{10}(\Delta h_m) + L_{ori} \tag{5}$$

The last term L_{ms} in (3) is determined by (6):

$$L_{ms} = L_{bsh} + k_a + k_d \cdot \log_{10}(d) + k_f \cdot \log_{10}(f_c) - 9 \cdot \log_{10}(b) \tag{6}$$

The term L_{bsh} in (6) is the shadowing gain that occurs when the GW antenna height h_{base} is higher than the building rooftops height h_{roof} and is given by (7):

$$L_{bsh} = \begin{cases} -18 \cdot \log_{10}\left(1 + \Delta_{h_{base}}\right), & \Delta_{h_{base}} > 0 \\ 0, & \Delta_{h_{base}} \leq 0 \end{cases} \tag{7}$$

The factor k_a in (6) can be determined by (8):

$$k_a = \begin{cases} 54, & \Delta_{h_{base}} > 0 \\ 54 + 0.8 \cdot |\Delta_{h_{base}}| & \Delta_{h_{base}} \leq 0, d \geq 0.5\ km \\ 54 + 0.8 \cdot |\Delta_{h_{base}}| \cdot \frac{d}{0.5}, & \Delta_{h_{base}} \leq 0, d < 0.5\ km \end{cases} \tag{8}$$

Journal of Microwaves, Optoelectronics and Electromagnetic Applications, Vol. 24, No. 3, e2025290613 Sep 2025
DOI: http://dx.doi.org/10.1590/2179-10742025v24i3290613

The factor k_d in (6) can be obtained by (9):

$$k_d = \begin{cases} 18, & \Delta_{h_{base}} > 0 \\ 18 + 15 \cdot \frac{|\Delta_{h_{base}}|}{h_{roof}}, & \Delta_{h_{base}} \leq 0 \end{cases} \quad (9)$$

And the factor k_f in (6) can be defined by (10):

$$k_f = -4 + \begin{cases} 0.7 \cdot \left(\frac{f_c}{925} - 1\right), & \text{medium city and suburban} \\ 1.5 \cdot \left(\frac{f_c}{925} - 1\right), & \text{metropolitan city} \end{cases} \quad (10)$$

where w is the street width, b is the distance between buildings, Δh_m is the difference between h_{roof} and the ED antenna height h_m, $\Delta_{h_{base}}$ is the difference between h_{base} and h_{roof}, all in meters, and L_{ori} in (6) is the correction factor in dB due to the angular difference in degrees between the street orientation and the incident wave propagation direction φ, and can be obtained by (11) [26]:

$$L_{ori} = \begin{cases} -10 + 0.354\varphi, & 0 \leq \varphi \leq 35°, \\ 2.5 + 0.075(\varphi - 35°), & 35° \leq \varphi \leq 55° \\ 4.0 - 0.114(\varphi - 55°), & 55° \leq \varphi \leq 90° \end{cases} \quad (11)$$

For the study region, w is 17.5 meters, b is 35 meters, h_{roof} is on average 4.5 meters and φ is considered as 90°. Also, h_{base} is 6 meters, h_m is 2 meters and f_c is 915 MHz.

B. OPNET Node Domain

In the OPNET node domain, the developed ED model (based on SX1276 [27]) is designed using OPNET's graphical process tool with a state diagram. As shown in Fig. 2(a), the model includes two radio components, LORA_PHY_TX (transmitter) and LORA_PHY_RX (receiver), for the PHY layer. The developed GW model (based on SX1301 [28]) uses six OPNET radio receiver components for the PHY layer, supporting up to eight frequency channels according to regional LoRaWAN parameters (AU915-928 MHz) and operating with $SF7$ to $SF12$. As shown in Fig. 2(b), the GW receivers, RX_SF7 to RX_SF12, connect to queue components, Q_SF7 to Q_SF12, allowing simultaneous reception of uplink packets on different SFs and frequency channels. The GATEWAY_EMAC component manages the forwarding of uplink packets to the NS.

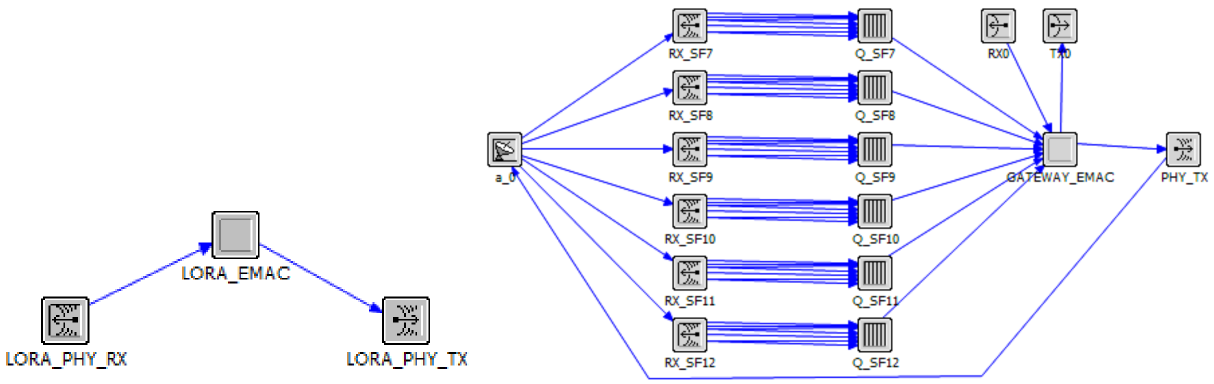

(a) (b)

Fig. 2. LoRaWAN models: (a) ED and (b) GW [29].

C. OPNET Process Domain

In the OPNET process domain, the developed LoRaWAN models utilize radio components where packet transmission is managed by pipelines that simulate the behavior of the radio link. These pipelines consist of multiple stages executed sequentially, encompassing the entire transmission process from the transmitting radio link to the receiving radio link. For LoRaWAN uplink models, the following OPNET radio transceiver pipeline stages were customized to accurately reflect the network's characteristics: *received-power*, *background-noise*, *signal-to-noise-ratio*, *interference-noise*, *bit-error-rate*, and *transmission-delay*.

In the *received-power* stage, the $P_{r_{dBm}}$ of the signal is given by (12):

$$P_{r_{dBm}} = P_{t_{dBm}} + G_{t_{dBi}} + G_{r_{dBi}} - L_{pr_{dB}} \tag{12}$$

where $G_{t_{dBi}}$ and $G_{r_{dBi}}$ represent the gains of the transmitting and receiving antennas, respectively, and $L_{pr_{dB}}$ is the path loss, which can be estimated by (2) and (3).

In the *background-noise* stage, the noise power $P_{n_{dB}}$ is given by (13):

$$P_{n_{dB}} = 30 \cdot \log_{10} \cdot [k_{TB} \cdot (T_r + T_{bk}) \cdot BW] \tag{13}$$

where T_{bk} is the equivalent background noise temperature, assumed to be 290 K, and T_r is the equivalent receiver noise temperature, which depends on the noise figure F and reference temperature T_0, as defined in (14):

$$T_r = (F - 1) \cdot T_0 \tag{14}$$

The power spectral density of ambient noise, which can represent sources as urban noise within the frequency band of interest, is considered negligible in this research and has therefore been disregarded.

In the *signal-to-noise ratio* stage, the ratio of the power of the desired signal to the weighted sum of the powers of the interfering signals is defined taking into account both the overlap time between each interfering packet and the desired packet, and the $P_{n_{dB}}$. Thus, the $SINR_{dB}$ can be defined by (15):

$$SINR_{dB} = 10 \cdot \log_{10} \left[\frac{P_{r_u}}{P_n + \sum_{i=1}^{N_{pktInt}} \left(P_i \cdot \frac{T_{i,overlap}}{T_u} \right)} \right] \tag{15}$$

where N_{pktInt} is the number of interfering packets, P_{r_u} is the power of the desired signal, P_i represents the power of the i-th interfering signal, $T_{i,overlap}$ is the overlap duration between the i-th interfering packet and the desired packet, and T_u is the total duration of the desired packet. In the *interference noise* stage, the interference power between the desired packet and the interfering packets is estimated considering that each interfering signal can be treated individually. Thus, if we analyze an example with three packets (A, B and C), where B is the desired packet and A and C are the interfering packets, each collision can be treated sequentially: $A{\rightarrow}B$, $C{\rightarrow}B$ and, then, $A{\rightarrow}C$. In this case, the power of the interfering signal in relation to the overlap time of packet $A{\rightarrow}B$ is summed and, at each overlap, that is, at each collision, the corresponding BER is calculated and the number of bit errors in B is accumulated.

In collision events, the degree of interference suffered by a packet as a function of SF can be estimated by the matrix of co-channel rejection coefficients, presented in (16) [30]. As can be seen, the rejection coefficient increases with SF, therefore, the higher the SF, the more resistant the packet is to interference. Thus, higher SF values are generally assigned to EDs further away from the GW, reducing the impact of interference caused by devices closer to the GW (usually received at a higher power level). In the event of a collision between packets with the same SF on the same frequency channel, the desired packet will not be discarded if its signal power is 6 dB higher than that of the interfering packet. However, in the case of different SFs, the desired packet will be processed if the difference between the signals exceeds the minimum required $SINR_{dB}$ value, as shown in Table I [13], [30].

$$\boldsymbol{M} = \begin{bmatrix} 6 & -16 & -18 & -19 & -19 & -20 \\ -25 & 6 & -20 & -22 & -22 & -22 \\ -27 & -27 & 6 & -23 & -25 & -25 \\ -30 & -30 & -30 & 6 & -26 & -28 \\ -33 & -33 & -33 & -33 & 6 & -29 \\ -36 & -36 & -36 & -36 & -36 & 6 \end{bmatrix} \quad (16)$$

Each element M_{ij} of (16) represents the minimum $SINR_{dB}$ required so that a collision between a desired packet with SF_i and an interfering packet with SF_j does not cause a packet drop. The indices i and j represent the row and column of the matrix, respectively, starting from the lowest value $SF7$ to the highest $SF12$, $i, j \in \{7, ..., 12\}$. The matrix elements were calculated considering complete overlap between signals, as observed in practical experiments with LoRa [13], [30].

In the *bit-error-rate* stage, the BER for AWGN and multipath fading channels as a function of $SINR_{dB}$ is determined for different SFs. For AWGN channels, the BER performance was obtained by the approximate closed-form expression (17) [31], [32] and the obtained results are presented in Fig. 3(a).

$$BER \approx 0.5 \cdot Q\left(\sqrt{SINR \cdot 2^{SF+1}} - \sqrt{1.386 \cdot SF + 1.154}\right) \quad (17)$$

where $Q(\cdot)$ is a function that represents the tail probability of the standard Gaussian distribution.

On the other hand, for multipath fading channels, the Rayleigh model was adopted and the BER performance was determined by equation (18) [32]. The corresponding results are presented in Fig. 3(b).

$$\begin{aligned} BER \approx 0.5 \cdot & \left[Q\left(-\sqrt{2 \cdot H_{2^{SF}-1}}\right) - \sqrt{\frac{2^{SF} \cdot SINR}{2^{SF} \cdot SINR + 1}} \cdot e^{-\frac{H_{2^{SF}-1}}{2^{SF} \cdot SINR + 1}} \right. \\ & \left. \cdot Q\left(\sqrt{\frac{2^{SF} \cdot SINR + 1}{2^{SF} \cdot SINR}} \cdot \left[-\sqrt{2 \cdot H_{2^{SF}-1}} + \frac{\sqrt{2 \cdot H_{2^{SF}-1}}}{2^{SF} \cdot SINR + 1}\right]\right)\right] \end{aligned} \quad (18)$$

where H_m can be approximately represented by $\ln(m) + \frac{1}{2m} + 0.57722$, with 0.57722 being the Euler–Mascheroni constant [32].

Comparing the results presented in Fig. 3(a) and Fig. 3(b) for a BW of 125 kHz and a target BER of $1 \cdot 10^{-4}$, LoRa can experience a $SINR_{dB}$ variation of more than 30 dB regardless of the SFs analyzed. This 30 dB link budget loss due to multipath fading results in a 13.9% reduction in network coverage, which can significantly impact the communication quality of LoRa in urban areas [32].

In the *transmission-delay* stage, the time-on-air ToA of the packet is computed as presented in (19) [33]:

$$ToA = T_{preamble} + T_{payload} \quad (19)$$

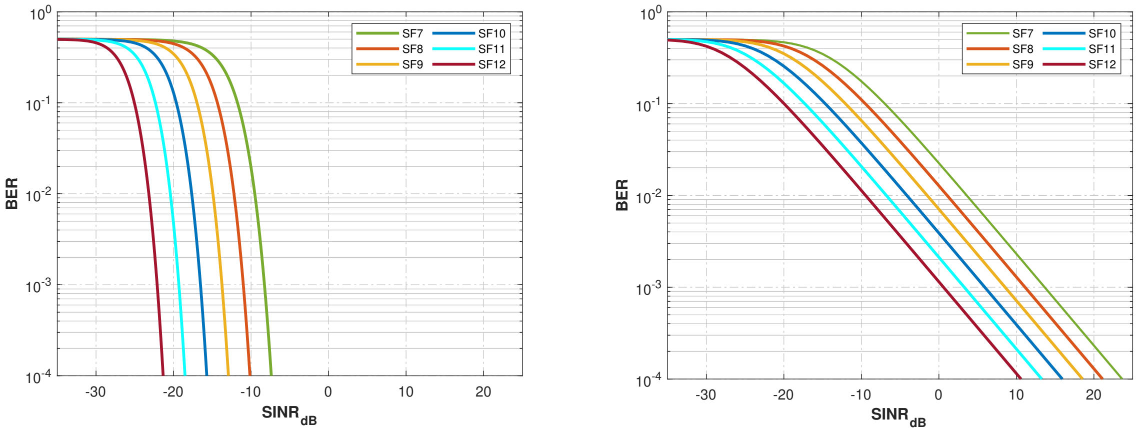

(a) (b)

Fig. 3. BER as a function of $SINR_{dB}$ for different SFs: (a) AWGN channel; (b) Multipath fading channel.

where $T_{preamble}$ represents the preamble duration and $T_{payload}$ is the payload duration, with $T_{preamble}$ being given by (20):

$$T_{preamble} = (N_{preamble} + 4.25) \cdot T_s \tag{20}$$

and with $T_{payload}$ being given by (21):

$$T_{payload} = N_{payload} \cdot T_s \tag{21}$$

where $N_{preamble}$ is the programmed preamble length (set to 8 for the AU915-928 MHz region) [34] and T_s is the symbol duration. $N_{payload}$ is the number of payload symbols, given by (22):

$$N_{payload} = 8 + \max\left(\left\lceil \frac{8 \cdot P_L - 4 \cdot SF + 28 + 16 \cdot I_{CRC} - 20 \cdot I_{IH}}{4 \cdot (SF - 2 \cdot I_{DE})} \right\rceil \cdot (cr + 4), 0\right) \tag{22}$$

where P_L is the number of payload bytes (1 to 255), I_{CRC} indicates the CRC (Cyclic Redundancy Check), with $I_{CRC} = 1$ for uplink and $I_{CRC} = 0$ for downlink. I_{IH} defines whether the header is present ($I_{IH} = 0$) or absent ($I_{IH} = 1$), and I_{DE} is used for increased transmission robustness [27].

A critical parameter related to the packet transmission rate is the duty cycle regulation in the ISM bands. After transmitting a packet, the device must wait T_{dc} seconds before transmitting again in the channel, according to (23) [18]:

$$T_{dc} = ToA \cdot \left(\frac{1}{d_c} - 1\right) \tag{23}$$

where d_c is the duty cycle factor dictated by regulatory constraints [18].

Another important performance parameter is the normalized throughput S, the ratio of successful data transmission to maximum data transmission capacity for each SF [35]. This normalized metric is used to provide the performance of the massive LoRaWAN uplink for different SFs and offered loads G. It is assumed that an ED generates a packet every Δt seconds, following a Poisson distribution, with each packet occupying the channel for ToA seconds. Therefore, S for each SF is defined by (24):

$$S = G \cdot R_{pkt} \tag{24}$$

where G represents the normalized offered loads for each SF, given by (25) [35], and R_{pkt} is the

Brazilian Microwave and Optoelectronics Society-SBMO received 25 Sep 2024; for review 15 OCt 2024; accepted 06 Apr 2025
Brazilian Society of Electromagnetism-SBMag ISSN 2179-1074

packet success probability for each SF, given by (26):

$$G = \frac{N_{pktTX} \cdot ToA}{T_{sim}} \tag{25}$$

$$R_{pkt} = \frac{N_{pktRX}}{N_{pktTX}} \tag{26}$$

where N_{pktTX} is the total number of transmitted packets for each SF, N_{pktRX} is the total number of successfully received packets for each SF, and T_{sim} is the simulation interval.

Additionally, the inter-frame delay D_{ifr} is the average delay between two consecutive successfully received packets at GW for each SF, and is given by (27):

$$D_{ifr} = \frac{1}{N_{pktRX}} \sum_{i=1}^{N_{pktRX}}, (t_i - t_{i-1}) \tag{27}$$

where t_i is the reception time of packet i, and t_{i-1} is the reception time of the preceding $i-1$.

The performance parameters S, R_{pkt}, and D_{ifr} depend on the packet collision rate R_{col}, BER, and GW sensitivity P_{GW}. Specifically, higher R_{col} and BER tend to reduce R_{pkt} and increase D_{ifr}. In this study, P_{GW} and $SINR_{dB}$ is defined based on the SX1301 specifications shown in Table I [28].

TABLE I. SOME SX1301 PARAMETERS AS A FUNCTION OF SF.

SF	P_{GW} (dBm)	ToA (ms)	$SINR_{dB}$ (dB)
7	-126.5	92.4	-7.5
8	-129.0	164.4	-10.0
9	-131.5	308.2	-12.5
10	-134.0	575.5	-15.0
11	-136.5	1232.9	-17.5
12	-139.5	2302.0	-20.0

D. Energy Consumption

One of the main constraints of IoT applications is the energy consumption of the ED [36]. The total energy consumed by the ED to transmit a packet over the LoRaWAN uplink is influenced by multiple factors, including the ED operational states, packet size, transmission current, which varies with $P_{t_{dBm}}$, and the ED operating voltage [36], [37].

The ED uplink operation consists of distinct states, including initialization, preparation, transmission, waiting, reception, processing, and shutdown [27], [37]. For example, Fig. 4 illustrates the sequence of states involved in transmitting a 51-byte packet using $SF12$ and Class A mode [36].

As observed in Fig. 4, state 1 (*wake up*) is responsible for activating the device from hibernation mode. In state 2 (*radio preparation*), the radio is prepared for transmission. State 3 (*transmission*) is dedicated to data transmission. In state 4 (*wait 1st window*), the device waits for the first reception window $RX1$. State 5 (*1st receive window*) is dedicated to data reception in $RX1$. State 6 (*wait 2nd window*) involves waiting for the second reception window $RX2$. In state 7 (*2nd receive window*), data reception occurs in $RX2$. State 8 (*radio off*) is responsible for turning off the radio. State 9 (*postprocessing*) deals with the processing of received or transmitted data. State 10 (*turn off sequence*) involves the device's shutdown sequence. Finally, state 11 (*sleep*) sets the device into hibernation mode to minimize energy consumption until the next activity cycle.

Brazilian Microwave and Optoelectronics Society-SBMO received 25 Sep 2024; for review 15 OCt 2024; accepted 06 Apr 2025
Brazilian Society of Electromagnetism-SBMag ISSN 2179-1074

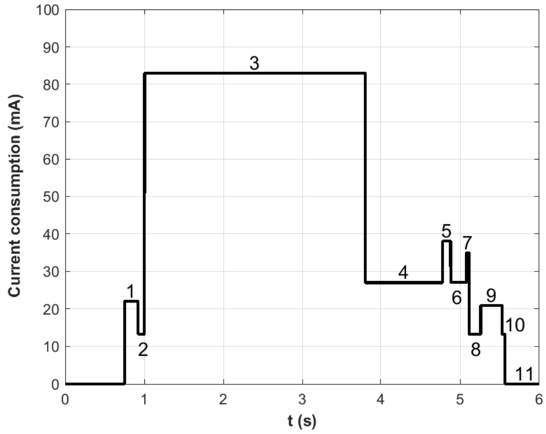

Fig. 4. LoRa uplink operation states.

The states 4, 5, 6 and 7 have been disabled to ensure an accurate evaluation of the uplink energy consumption. This approach reflects the operational scenario in which the ED acts only on the uplink, without receiving any packets from the NS (via the GW). Therefore, in this research, only the following related uplink states of the ED are analyzed: *wake up*, *radio preparation*, *transmission*, *radio off*, *switch off sequence* and *sleep*. In sleep mode, the sleep time T_{sleep} is given by (28):

$$T_{sleep} = \Delta t - T_{act} \tag{28}$$

where Δt is the time interval between two consecutive periodic packet transmissions performed by the ED, and T_{act} is the total duration of the activity states of the device. More precisely, T_{act} is the sum of the times for waking up T_{wu}, preparing the radio T_{pre}, transmitting T_{tx}, turning off the radio T_{off} and for the shutdown sequence T_{seq}, as shown in (29):

$$T_{act} = T_{wu} + T_{pre} + T_{tx} + T_{off} + T_{seq} \tag{29}$$

The energy E_i consumed by the ED in state i is determined by (30):

$$E_i = T_i \cdot I_i \cdot V_{ED} \tag{30}$$

where T_i is the time duration of state i, I_i is the average current consumed in state i, and V_{ED} is the nominal operating voltage of the ED.

Therefore, the total energy consumption E_{total} is given by (31):

$$E_{total} = \sum_{i=1}^{N_{states}} E_i \tag{31}$$

where N_{states} represents the number of states. Table II presents the duration and average current associated with each of the states that make up T_{act}.

The device´s lifespan can be estimated using $\frac{C_B}{E_{day}}$ [38], where E_{day} is the average daily energy consumption and C_B is the total battery capacity, assumed to be 1000 mAh (equivalent to 11880 J at V_{ED} = 3.3 V). However, it is important to note this parameter offers only an approximation of the device's actual lifespan, as factors such as environmental conditions, usage patterns, and battery quality can significantly influence the battery's performance over time.

  ISSN 2179-1074

TABLE II. SX1276 CURRENT MEASUREMENTS @ $BW = 125$ KHZ (PA_BOOST + HIGH POWER OPERATION) [27].

State	Symb	ms	Symb	mA
wake up	T_{wu}	168.2	I_{wu}	22.1
radio preparation	T_{pre}	83.8	I_{pre}	13.3
transmission	T_{tx}	ToA (Tab. I)	I_{tx}	105
radio off	T_{off}	147.4	I_{off}	13.2
turn off sequence	T_{seq}	38.6	I_{seq}	13.3
sleep	T_{sleep}	Δt - T_{act}	I_{sleep}	$1 \cdot 10^{-7}$

V. ANALYSIS OF RESULTS

In this section, the performance of the multichannel P-ALOHA protocol of the uplink of the massive LoRaWAN under study will be investigated for Scenario-1 and Scenario-2 for different SF. The following performance parameters are analyzed: S, BER, R_{col}, R_{pkt}, and D_{ifr}. For the energy consumption analysis, the energy cost per transmitted bit E_{bTX} and energy efficiency per received bit E_{bRX} are also evaluated.

Without loss of generality, when not stated, the analyses will focus on the condition of maximum S. The Δt values that correspond to the maximum S for different SFs are referred to Δt_{REF} (i.e. the reference Δt). For each performance parameter analyzed, 23 sequential simulations are performed, varying Δt from approximately $1 \cdot 10^0$ to $1 \cdot 10^3$ seconds.

A. Throughput

In Fig. 5, the simulation results of S as a function of G of the analyzed LoRaWAN uplink for different SFs (distributed in sectors as shown in Fig. 1) are presented for (a) Scenario-1 and (b) Scenario-2. It can be observed that S tends to increase as G increases until a saturation point, where S is maximum. After this point, increasing G causes a drastic reduction in S due to increased packet loss.

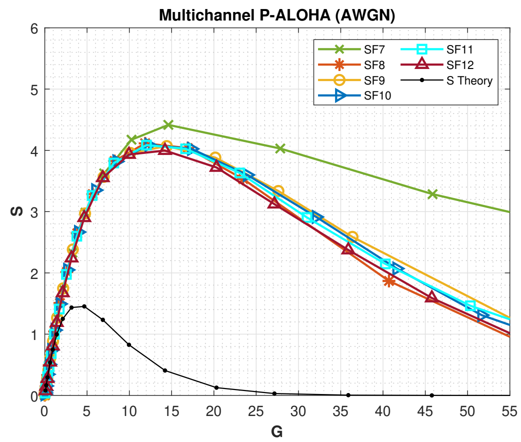

(a)

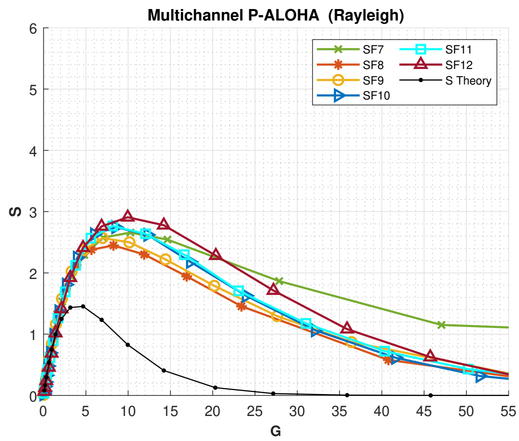

(b)

Fig. 5. S as a function of G for differentSFs: (a) Scenario-1, (b) Scenario-2.

As shown in Fig. 5 (a), for Scenario-1, there is a significant increase in S for different SFs compared to the theoretical multichannel P-ALOHA protocol. The theoretical S for the multichannel P-ALOHA protocol is defined as $S = G \cdot e^{-\frac{2G}{N_{ch}}}$, where N_{ch} is the number of available channels [19]. For $SF7$, the

  ISSN 2179-1074

maximum S is 3.2 times higher, reaching 4.5, while for other SFs, the increase is around 2.8 times, reaching 4.0. This gain can be attributed to the reduction of load and interference in each channel provided by the use of LoRa modulation (orthogonality between signals with different SFs) and FCH (pseudo-randomness of channel selection in each transmission) in the LoRaWAN uplink. It can be noticed that S reaches similar maximum values for all SFs, with $SF7$ standing out for its superior performance. This result is attributed to the lower ToA of $SF7$, which reduces the channel occupancy, decreases the R_{col} and increases the effective R_b, although at the cost of a reduction in the transmission range. In contrast, although operating at greater distances from GW, the other SFs provide robustness to interference and keep similar S, with only small variations as G increases.

However, as shown in Fig. 5(b), due to the severe propagation conditions, S is significantly lower in Scenario-2 than in Scenario-1 for all SFs. Performance degradation is mainly caused by multipath fading, which increases the BER and reduces the effective R_b, with the increase in BER being most noticeable for $SINR_{dB}$ below 22 dB for $SF7$ and below 10 dB for $SF12$, as shown in Fig. 3(b).

Table III presents the maximum S for Scenarios-1 and Scenarios-2. It can be observed that S is 4.08 for Scenario-1, while it is 2.6 for Scenario-2. This indicates that, compared to Scenario-1, there was a S reduction in Scenario-2 of approximately 35.5%. Therefore, the LoRaWAN uplink transmission efficiency drops significantly in the presence of multipath fading, even with all its mechanisms to increase robustness to adverse channel conditions.

TABLE III. MAXIMUM S FOR DIFFERENT SFs.

	SF7	***SF8***	***SF9***	***SF10***	***SF11***	***SF12***
Scenario-1	4.4	4.1	4.0	4.0	4.0	4.0
Scenario-2	2.6	2.4	2.5	2.7	2.7	2.9

As a result, the performance of S in Fig. 5(a) and Fig. 5(b) exhibits strong consistency with the results in Fig. 2 of [39], where S was evaluated through simulations and theoretical analyzes under conditions of perfect and imperfect orthogonality between SFs for a variable number of EDs transmitting simultaneously. Notably, S aligns with the trends reported in [39] for inter-SF and intra-SF interference under imperfect orthogonality.

B. Bit Error Rate

In Fig. 6, the simulation results of BER as a function of Δt for the analyzed LoRaWAN uplink for different SFs are shown, considering (a) Scenario-1 and (b) Scenario-2. It can be seen that when $SINR_{dB}$ drops below the thresholds indicated in Table I, packet reception deteriorates, leading to a higher packet loss rate and a reduction in communication efficiency. This is exacerbated in Scenario-2, where channel variation and signal loss are more pronounced.

As shown in Fig. 6(a), for Scenario-1, the observed BER was low, with most of the transmissions received by the GW presenting a BER below $1 \cdot 10^{-8}$. By analyzing the results for all SFs, it can be seen that the average BER variations are not significant. The main factor affecting the uplink performance of the network in this scenario was the collisions between the transmitted packets.

However, as shown in Fig. 6(b), for Scenario-2, the BER values are higher due to the more severe channel conditions. The BER results in Scenario-2 range from $8.4 \cdot 10^{-4}$ for $SF7$ to $1.03 \cdot 10^{-3}$ for

Brazilian Microwave and Optoelectronics Society-SBMO received 25 Sep 2024; for review 15 OCt 2024; accepted 06 Apr 2025
Brazilian Society of Electromagnetism-SBMag ISSN 2179-1074

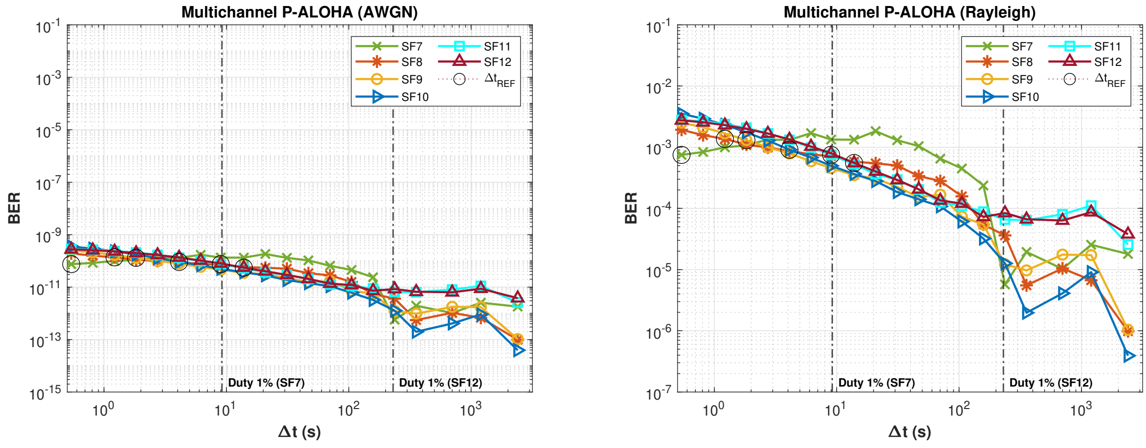

(a) (b)

Fig. 6. BER as a function of Δt for different SFs: (a) Scenario-1, (b) Scenario-2.

$SF12$. Additionally, it can be observed that the BER increases slightly with increasing SF, especially from $SF10$ onwards.

When comparing the results for Scenario-1 and Scenario-2, it can be verified that the adverse conditions of Scenario-2 significantly impact the BER for all SFs. Considering a duty cycle of 1%, for Scenario-1, the BER values ranged from $1.3 \cdot 10^{-10}$ for $SF7$ to $8.3 \cdot 10^{-12}$ for $SF12$. On the other hand, for Scenario-2, the BER values are significantly higher, ranging from $1.3 \cdot 10^{-3}$ for $SF7$ to $8.1 \cdot 10^{-5}$ for $SF12$. This further implies that the error rates increase as SF decreases.

C. Collision Rate

Fig. 7 shows the simulation results of R_{col} as a function of Δt for different SFs, considering Scenario-1 and Scenario-2. It can be observed that, as Δt decreases, packet collisions increase, since G is inversely proportional to Δt.

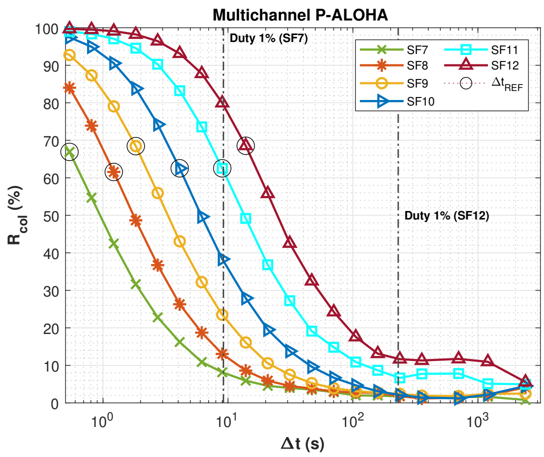

Fig. 7. R_{col} (%) as a function of Δt for different SFs.

As mentioned, collisions are primarily driven by two factors: the first occurs when two packets are received simultaneously on the same frequency channel with the same SF. In this case, the packets with a signal power at least 6 dB higher than the other will be processed; otherwise, both packets will be lost. The second factor involves collisions between packets with different SFs transmitted on the same frequency channel. For successful reception, the stronger signal must exceed the minimum required $SINR_{dB}$ for the respective SF as specified in (16).

Therefore, since the R_{col} is determined by these factors, in the model developed, the impact of fading on collisions is considered negligible. Thus, in both Scenarios, the R_{col} as a function of Δt_{REF} for the different SFs is 65%. The R_{col} for each SF are provided in Table IV.

TABLE IV. R_{col} (%) AS A FUNCTION OF Δt_{REF} FOR DIFFERENT SFs.

	SF7	***SF8***	***SF9***	***SF10***	***SF11***	***SF12***
Scenario-1 and Scenario-2	66.9	61.5	68.4	62.5	62.5	68.5
Δt_{REF} **(s)**	0.5	1.2	1.8	4.1	9.0	13.8

Similarly, under a 1% duty cycle, the R_{col} remains consistent at 8.86%, as shown in Table V. Therefore, these results indicate that packet collisions are one of the main factors limiting the uplink performance of a massive LoRaWAN, becoming more frequent as more devices try to transmit on the same frequency channel, especially when using higher SFs.

TABLE V. R_{col} (%) AS A FUNCTION OF Δt_{REF} (1% DUTY CYCLE) FOR DIFFERENT SFs.

	SF7	***SF8***	***SF9***	***SF10***	***SF11***	***SF12***
Scenario-1 and Scenario-2	8.0	7.6	7.6	8.2	10.1	11.7
Δt_{REF} **(s)**	9.2	16.4	30.8	57.5	123.3	230.2

D. Successfully Received Packet Rate

In Fig. 8, the simulation results of R_{pkt} as a function of Δt of the LoRaWAN uplink are shown for different SFs, considering (a) Scenario-1 and (b) Scenario-2.

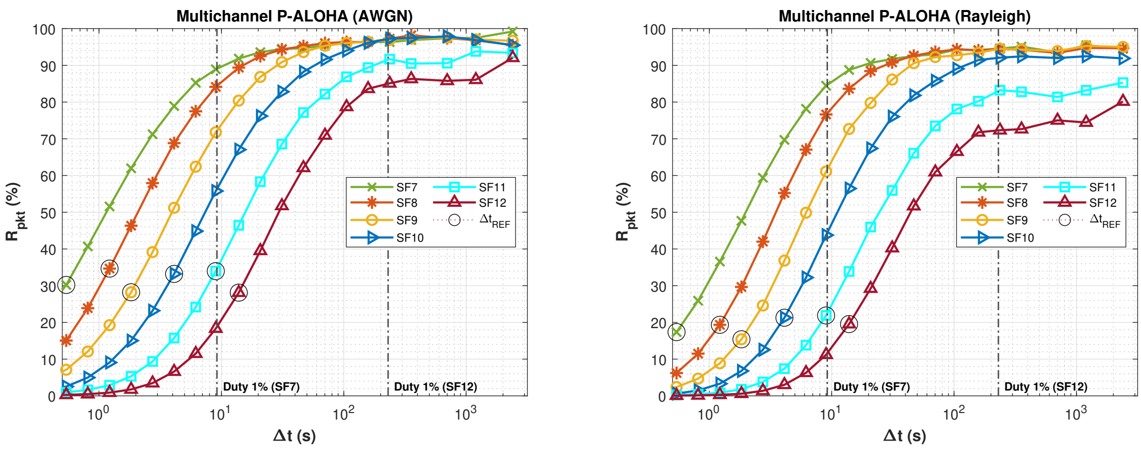

(a) (b)

Fig. 8. R_{pkt} (%) as a function of Δt for different SFs: (a) Scenario-1, (b) Scenario-2.

As shown in Fig. 8(a), for Scenario-1, R_{pkt} is 31.3%, presenting a notable performance drop as Δt decreases. This implies that packet collisions negatively impact R_{pkt}. It is also observed that for a duty cycle of 1%, the value of R_{pkt} for different SFs is 88.75%. Hence, R_{pkt} is 68.7% for S maximum and 11.25% for a duty cycle of 1%.

ISSN 2179-1074

On the other hand, as shown in Fig. 8(b), for Scenario-2, R_{pkt} is lower, reaching 19.13%. This implies that R_{pkt} is approximately 81.87% for S maximum and 81.7% for a duty cycle of 1%. These results indicate the negative impacts of packet collisions and multipath fading on BER for Scenario-2.

Table VI shows the results of R_{pkt} as a function of Δt_{REF} for different SFs, considering the two scenarios analyzed. Comparing the R_{pkt} results for Scenario-1 and Scenario-2, as shown in Table VI, it can be observed that Scenario-2 causes an average reduction of 38.9% when S is maximum and a reduction of 7.94% for 1% duty cycle. This decrease is attributed to the effects of multipath fading on BER, which affects signal quality and increases the probability of reception errors.

TABLE VI. R_{pkt} (%) AS A FUNCTION OF Δt_{REF} FOR DIFFERENT SFs.

	SF7	***SF8***	***SF9***	***SF10***	***SF11***	***SF12***
Scenario-1	30.2	34.6	28.2	33.2	33.9	28,1
Scenario-2	17.36	19.34	15.4	21.27	21.89	19.54
Δt_{REF} (s)	1.2	2.7	4.1	9.0	13.8	31.2

Table VII presents the R_{pkt} values as a function of Δt_{REF} for different SFs under a 1% duty cycle in both Scenarios 1 and 2. It can be seen that the highest SFs are those with the lowest R_{pkt}.

TABLE VII. R_{pkt} (%) AS A FUNCTION OF Δt_{REF} (1% DUTY CYCLE) FOR DIFFERENT SFs.

	SF7	***SF8***	***SF9***	***SF10***	***SF11***	***SF12***
Scenario-1	89.0	90.5	90.7	89.7	87.7	84.9
Scenario-2	84.6	85.3	85.8	83.6	78.8	72.2
Δt_{REF} (s)	9.2	16.4	30.8	57.5	123.3	230.2

E. Delay Inter-Frame Rate

Fig. 9 shows the simulation results of the analyzed LoRaWAN uplink D_{ifr} as a function of Δt for different SFs, considering (a) Scenario-1 and (b) Scenario-2. It is observed that as Δt decreases, D_{ifr} increases for all SFs, with this effect being more pronounced for higher SFs. This increase is mainly due to frequent destructive packet collisions.

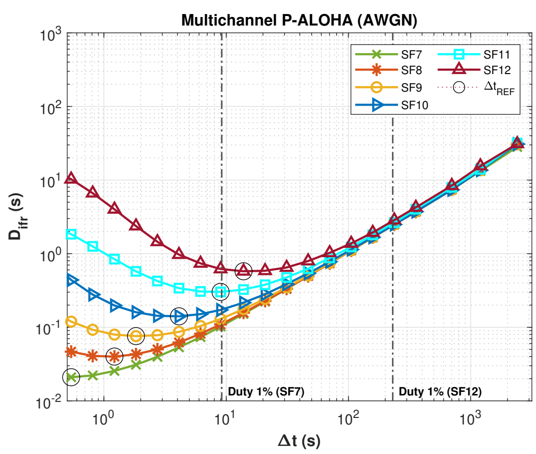

(a)

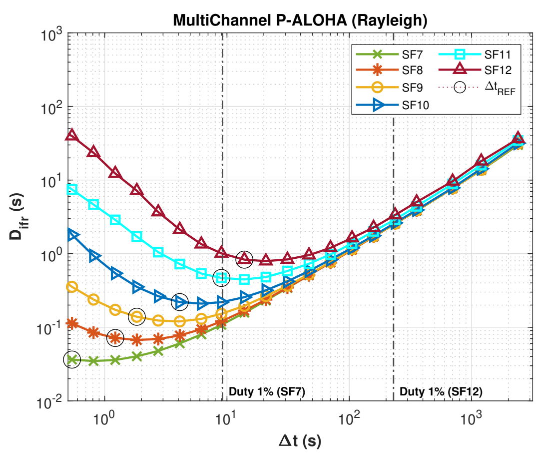

(b)

Fig. 9. D_{ifr} (s) as a function of Δt for different SFs: (a) Scenario-1, (b) Scenario-2.

  ISSN 2179-1074

For example, as shown in Fig. 9(a), for Scenario-1, when S is maximum, D_{ifr} ranges from 0.02 to 0.57 seconds, with the smallest variation for $SF7$ and the largest for $SF12$. An important factor to consider is the relationship between D_{ifr} and R_{pkt}. When D_{ifr} is reduced, R_{pkt} increases, resulting in higher S. Therefore, after network saturation, D_{ifr} is significantly higher.

On the other hand, as shown in Fig. 9(b), for Scenario-2, the same trend is observed but the increase in D_{ifr} is even more evident due to the impact of multipath fading on BER. Therefore, when S is maximum, D_{ifr} varies from 0.03 to 0.82 seconds, with the smallest variation for $SF7$ and the largest for $SF12$, indicating higher latency, particularly for $SF12$, where the distances to the GW is greater and collisions are more destructive due to the longer ToA and higher channel occupancy.

As a result, the comparison between the analyzed Scenarios reveals that multipath fading increases the average D_{ifr} by approximately 80% for $SF7$ and 43% for $SF12$, exacerbating the latency issues as the Δt decreases.

F. Energy Cost Analysis

This subsection evaluates E_{bTX} and E_{bRX} to provide an assessment of the energy cost of the analyzed massive LoRaWAN uplink. Energy cost is an important parameter to estimate the battery life of EDs and evaluate the efficiency of the multichannel P-ALOHA protocol in the network [36].

The E_{bTX} of the LoRaWAN uplink can be determined from the $E_{total_{tx}}$ spent during T_{sim} for each SF, as described by (32):

$$E_{bTX} = \frac{E_{total_{tx}}}{N_{bits_{tx}}} \tag{32}$$

where $N_{bits_{tx}}$ is the number of bits transmitted for each SF observed during T_{sim}. Table VIII shows the average E_{bTX}, expressed in mJ/bit, for different SFs and scenarios.

TABLE VIII. AVERAGE E_{bTX} (MJ/BIT) FOR DIFFERENT SFs.

	SF7	***SF8***	***SF9***	***SF10***	***SF11***	***SF12***
Scenarios 1 and Scenario-2	0.152	0.220	0.355	0.607	1.22	2.23

The E_{bRX} considers the $E_{total_{tx}}$ for each SF during the T_{sim}, in relation to the number of bits successfully received $N_{bits_{rx}}$ at the GW. This parameter captures inefficiencies in the transmission process, such as losses caused by collisions or interference, allowing their impact to be evaluated. E_{bRX} is given by (33):

$$E_{bRX} = \frac{E_{bTX} \cdot N_{bits_{tx}}}{N_{bits_{rx}}} = \frac{E_{total_{tx}}}{N_{bits_{rx}}} \tag{33}$$

Fig. 10, shows the simulation results of the analyzed LoRaWAN uplink E_{bRX} as a function of Δt for different SFs, considering (a) Scenario-1 and (b) Scenario-2. It is observed that as Δt decreases, E_{bRX} increases for all SFs, with this effect being more pronounced for higher SFs. This increase is mainly due to frequent destructive packet collisions. Additionally, the analysis shows that the choice of SFs directly impacts E_{bRX}.

For instance, as shown in Fig. 10(a) and Fig. 10(b), $SF12$ incurs a slightly higher energy cost than $SF10$ due to its lower R_b, leading to longer transmission times. Since higher SF values increase the ToA, they occupy the channel for extended periods, raising the risk of collisions among concurrent LoRa packets. This results in interference, degrading the transmission quality and increasing the E_{bRX} for larger SF. These observations align with the trends shown in Fig. 18 and Fig. 19 of [36].

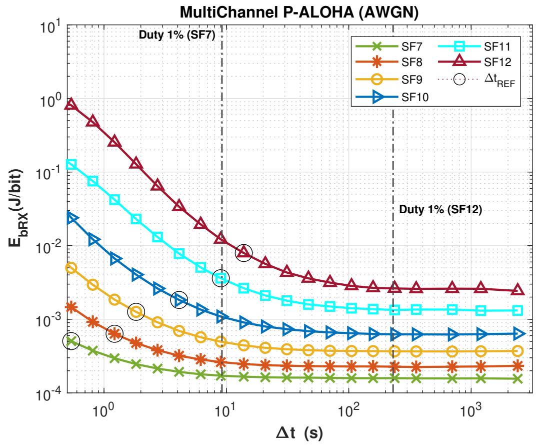

(a)

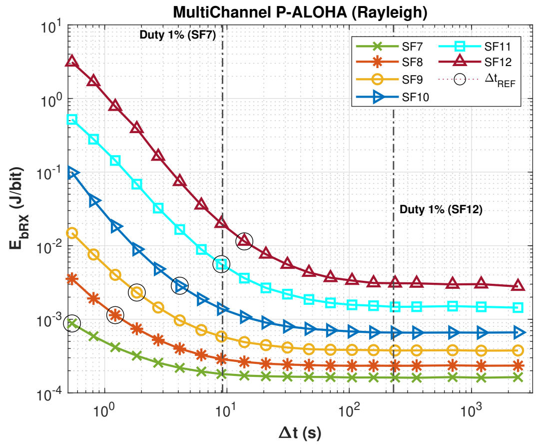

(b)

Fig. 10. E_{bRX} (J/bit) as a function of Δt for different SFs: (a) Scenario-1, (b) Scenario-2.

On the other hand, as shown in Table VIII, for Scenario-1, the average E_{bRX} ranges from 0.5044 mJ/bit to 7.943 mJ/bit for S maximum, with the smallest variation for $SF7$ and the largest for $SF12$. This indicates that EDs configured with $SF7$ are more energy efficient.

As shown in Table VIII, for Scenario-2, the average E_{bRX} ranges from 0.877 mJ/bit for $SF7$ to 11.42 mJ/bit for $SF12$, demonstrating that multipath fading increases the E_{bRX}. Note that the average E_{bRX} is achieved for $SF7$ at a R_b of 10.59 kbps and for $SF12$ at a rate of 0.464 kbps. As a result, the comparison between the analyzed scenarios shows that multipath fading increases the average E_{bRX} by approximately 57% for $SF7$ and 69% for $SF12$, exacerbating the latency issues as the SF increases.

TABLE IX. AVERAGE E_{bRX} (MJ/BIT) AS A FUNCTION OF Δt_{REF} FOR DIFFERENT SFs.

	SF7	*SF8*	*SF9*	*SF10*	*SF11*	*SF12*
Scenario-1	0.504	0.635	1.26	1.828	3.609	7.943
Scenario-2	0.877	1.138	2.308	2.854	5.601	11.42
Δt_{REF} (s)	1.2	2.7	4.1	9.0	13.8	31.2

To illustrate the practical impact, with an average E_{bRX} of 0.5044 mJ/bit in $SF7$, operating at a R_b of 17.587 kbps, the battery life is approximately 1.54 days. In contrast, for $SF12$, with an average E_{bRX} of 7.943 mJ/bit and operating at a rate of 0.638 kbps, the battery life is longer, reaching approximately 2.7 days. Considering a duty cycle of 1%, the battery life of the ED operating at $SF7$ with a R_b of $3.549 \cdot 10^{-3}$ kbps is approximately 22.7 days. In contrast, the battery life for $SF12$ at a rate of $0.134 \cdot 10^{-3}$ kbps is approximately 39.5 days.

Therefore, for a Δt_{REF}, an average E_{bRX} greater than an average E_{bTX} means that a significant amount of energy is wasted. This waste can occur due to collisions and interference caused by the low efficiency of the P-ALOHA protocol.

VI. WASTED ENERGY ANALYSIS

In this section, the wasted energy E_w of the uplink of the massive LoRaWAN under study is deeper analyzed. This parameter is important for identifying the impact of transmission losses on the network, considering variations in Δt.

To calculate E_w, E_{bTX} and E_{bRX} data are first linearly interpolated to ensure that both functions are defined at the same Δt points. The area is then calculated by integrating the difference between the curves (the difference in energy) over time as Δt increases. The integral of the difference between the curves is calculated using the trapezoidal rule. The energy consumption for 1 hour of operation in LoRaWAN is then calculated for each SF, and then the average battery life is estimated. On the other hand, the area between the curves of E_{bTX} and E_{bRX} as a function of Δt represents the E_w of packets that were not successfully received at the GW during T_{sim} for each SF.

Fig. 11 shows the simulation results of the analyzed LoRaWAN uplink E_w as a function of Δt for $SF7$ and $SF12$, considering (a) Scenario-1 and (b) Scenario-2. It is observed that as Δt decreases, E_w increases for all SFs, with this effect being more pronounced for higher SFs. This increase is mainly due to frequent destructive packet collisions.

As a result, the comparison between the analyzed SFs for Scenario-1 (Fig. 11(a)) shows that the average E_w for $SF7$ is approximately 938.40 J/h, while for $SF12$ it reaches 7078.21 J/h, indicating an increase of about 654.28%. This substantial increase in E_w highlights how higher SFs significantly exacerbate E_w in the network.

Fig. 11(b), for Scenario-2, shows that the E_w for each SF is significantly higher compared to Scenario-1. Specifically, for Scenario-2, the average E_w for $SF7$ is 2996.62 J/h and for $SF12$ is 12291.99 J/h. This significant increase is mainly due to the multipath fading adopted in Scenario-2, which introduces multipath effects. As a result, as Δt decreases, packet losses become more frequent, increasing E_w and directly affecting network efficiency.

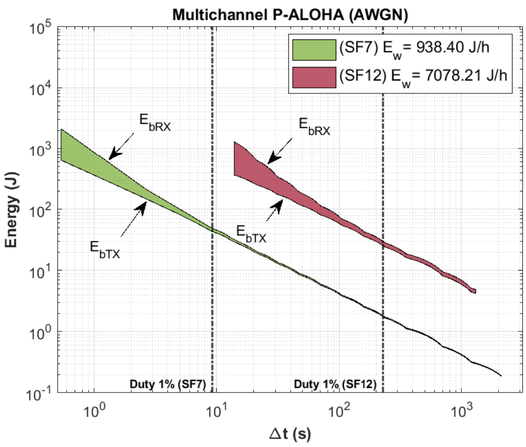

(a)

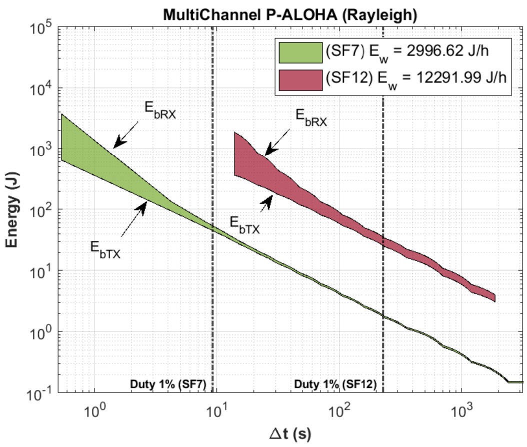

(b)

Fig. 11. Average E_w (J) as a function of Δt for $SF7$ and $SF12$: (a) Scenario-1, (b) Scenario-2.

To illustrate the practical impact of these results, for Scenario-1, the average E_w for $SF7$ corresponds to approximately 0.079 hours of battery life, while for $SF12$, this value rises to approximately 0.595 hours. For Scenario-2, the average E_w for $SF7$ corresponds to approximately 0.25 hours of battery life, while for $SF12$, this value rises to approximately 1.03 hours.

VII. Conclusion

In this work, the performance of the uplink of a massive LoRaWAN operating with the multichannel P-ALOHA protocol was analyzed using computational models developed in OPNET Modeler. Simulations were performed considering the propagation losses given by the COST231-WI model, as well as the effect of AWGN and multipath fading channels on the communication links, to determine the network performance. This approach allowed a systematic evaluation of key performance metrics, such as throughput, error rate, delay and energy consumption in a given coverage area.

The results show a critical trade-off when using higher SFs for uplink in a massive LoRaWAN. The analysis showed that for Scenario-1, E_w is about 7.5 times higher for $SF12$ than for $SF7$, while for Scenario-2, E_w is about 4.1 times higher. Analyzing also the trade-off between E_w and communication distance, it can be seen that in Scenario-1 the E_w per meter for $SF7$ is 7.5 J/h/m (Joule/hour/meter) and for $SF12$ it is 9.42 J/h/m. For Scenario-2, the E_w per meter is 23.97 J/h/m for $SF7$ and 16.38 J/h/m for $SF12$.

Therefore, the trade-off highlights the need for careful SF selection in LoRaWAN uplink deployments, balancing energy efficiency with the desired range. While higher SFs enable longer communication distances, they come at the cost of significantly increased energy consumption, which can be a limiting factor in battery-powered devices. In conclusion, while multichannel P-ALOHA provides a simple and energy-efficient access method, its scalability is constrained by network density and environmental factors.

VIII. Acknowledgment

This research was partially supported by the Instituto Nacional de Ciência e Tecnologia em Energia Elétrica (INERGE), Conselho Nacional de Desenvolvimento Científico e Tecnológico (CNPq), Coordenação de Aperfeiçoamento de Pessoal de Nível Superior (CAPES) under Grant 001, and Fundação de Amparo à Pesquisa do Estado de São Paulo (FAPESP) under Grants 2022/08737-1 and 2022/10876-0.

References

[1] S. Devalal and A. Karthikeyan, "LoRa Technology - An Overview," in *2018 Second International Conference on Electronics, Communication and Aerospace Technology (ICECA)*, pp. 284–290, 2018, DOI: 10.1109/ICECA.2018.8474715.

[2] R. Muppala, A. Navnit, S. Poondla, and A. M. Hussain, "Investigation of Indoor LoRaWAN Signal Propagation for Real-World Applications," in *2021 6th International Conference for Convergence in Technology (I2CT)*, pp. 1–5, 2021, DOI: 10.1109/I2CT51068.2021.9418173.

[3] L. Feltrin, C. Buratti, E. Vinciarelli, R. De Bonis, and R. Verdone, "LoRaWAN: Evaluation of Link and System Level Performance," *IEEE Internet of Things Journal*, vol. 5, no. 3, pp. 2249–2258, 2018, DOI: 10.1109/JIOT.2018.2828867.

[4] G. Boquet, P. Tuset-Peiró, F. Adelantado, T. Watteyne, and X. Vilajosana, "LR-FHSS: Overview and Performance Analysis," *IEEE Communications Magazine*, vol. 59, no. 3, pp. 30–36, 2021, DOI: 10.1109/MCOM.001.2000627.

[5] P. S. Cheong, J. Bergs, C. Hawinkel, and J. Famaey, "Comparison of LoRaWAN Classes and Their Power consumption," in *2017 IEEE Symposium on Communications and Vehicular Technology (SCVT)*, pp. 1–6, 2017, DOI: 10.1109/SCVT.2017.8240313.

[6] F. Van den Abeele, J. Haxhibeqiri, I. Moerman, and J. Hoebeke, "Scalability Analysis of Large Scale LoRaWAN Networks in NS-3," *IEEE Internet of Things Journal*, vol. 4, no. 6, pp. 2186–2198, 2017, DOI: 10.1109/JIOT.2017.2768498.

[7] M. Alenezi, K. K. Chai, Y. Chen, and S. Jimaa, "Ultra-dense LoRaWAN: Reviews and Challenges," *IET Communications*, vol. 14, no. 9, pp. 1361–1371, 2020, DOI: 10.1049/iet-com.2018.6128.

[8] D. Bankov, E. Khorov, and A. Lyakhov, "On the Limits of LoRaWAN Channel Access," in *2016 International Conference on Engineering and Telecommunication (EnT)*, pp. 10–14, 2016, DOI: 10.1109/EnT.2016.011.

[9] A. Rahmadhani and F. Kuipers, "When LoRaWAN Frames Collide," in *Proceedings of the 12th International Workshop on Wireless Network Testbeds, Experimental Evaluation & Characterization*, p. 89–97, 2018, DOI: 10.1145/3267204.3267212.

[10] R. Fujdiak, P. Mlynek, J. Misurec, and M. Strajt, "Simulated Coverage Estimation of Single Gateway LoRaWAN Network," in *2018 25th International Conference on Systems, Signals and Image Processing (IWSSIP)*, pp. 1–4, 2018, DOI: 10.1109/IWSSIP.2018.8439232.

[11] Z. Lu and H. Yang, *Unlocking the Power of OPNET Modeler*. Cambridge University Press, 2012.

[12] A. D. Jun, S. Hong, W. Lee, K. Lee, I. Joe, K. Lee, and T.-J. Park, "Modeling and Simulation of LoRa in OPNET," in *Advanced Multimedia and Ubiquitous Engineering*, pp. 551–559, 2017, DOI: 10.1007/978-981-10-5041-1_88.

[13] J. Markkula, K. Mikhaylov, and J. Haapola, "Simulating LoRaWAN: On Importance of Inter Spreading Factor Interference and Collision Effect," in *ICC 2019 - 2019 IEEE International Conference on Communications (ICC)*, pp. 1–7, 2019, DOI: 10.1109/ICC.2019.8761055.

[14] A. Hoeller, J. Sant'Ana, J. Markkula, K. Mikhaylov, R. Souza, and H. Alves, "Beyond 5G Low-Power Wide-Area Networks: A LoRaWAN Suitability Study," in *2020 2nd 6G Wireless Summit (6G SUMMIT)*, pp. 1–5, 2020, DOI: 10.1109/6GSUMMIT49458.2020.9083800.

[15] A. Hoeller, R. D. Souza, H. Alves, O. L. Alcaraz López, S. Montejo-Sánchez, and M. E. Pellenz, "Optimum LoRaWAN Configuration Under Wi-SUN Interference," *IEEE Access*, vol. 7, pp. 170 936–170 948, 2019, DOI: 10.1109/ACCESS.2019.2955750.

[16] D. Croce, M. Gucciardo, S. Mangione, G. Santaromita, and I. Tinnirello, "Impact of LoRa Imperfect Orthogonality: Analysis of Link-Level Performance," *IEEE Communications Letters*, vol. 22, no. 4, pp. 796–799, 2018, DOI: 10.1109/LCOMM.2018.2797057.

[17] M. A. Ertürk, M. A. Aydın, M. T. Büyükakkaşlar, and H. Evirgen, "A Survey on LoRaWAN Architecture, Protocol and Technologies," *Future Internet*, vol. 11, no. 10, 2019, DOI: 10.3390/fi11100216.

[18] F. Adelantado, X. Vilajosana, P. Tuset-Peiro, B. Martinez, J. Melia-Segui, and T. Watteyne, "Understanding the Limits of LoRaWAN," *IEEE Communications Magazine*, vol. 55, no. 9, pp. 34–40, 2017, DOI: 10.1109/MCOM.2017.1600613.

[19] D. T. C. Wong, Q. Chen, X. Peng, and F. Chin, "Performance Analysis of Multi-Channel Pure Collective Aloha MAC Protocol for Satellite Uplink Access," in *TENCON 2017 - 2017 IEEE Region 10 Conference*, pp. 164–169, 2017, DOI: 10.1109/TENCON.2017.8227855.

[20] U. Raza, P. Kulkarni, and M. Sooriyabandara, "Low Power Wide Area Networks: An Overview," *IEEE Communications Surveys & Tutorials*, vol. 19, no. 2, pp. 855–873, 2017, DOI: 10.1109/COMST.2017.2652320.

[21] G. Baruffa, L. Rugini, V. Mecarelli, L. Germani, and F. Frescura, "Coded LoRa Performance in Wireless Channels," in *2019 IEEE 30th Annual International Symposium on Personal, Indoor and Mobile Radio Communications (PIMRC)*, pp. 1–6, 2019, DOI: 10.1109/PIMRC.2019.8904298.

[22] T. Elshabrawy and J. Robert, "Evaluation of the BER Performance of LoRa Communication using BICM Decoding," in *2019 IEEE 9th International Conference on Consumer Electronics (ICCE-Berlin)*, pp. 162–167, 2019, DOI: 10.1109/ICCE-Berlin47944.2019.8966172.

[23] E. Silva and F. S. Sousa, "Sistema Inteligente de Alerta de Enxurrada por Rede LoRa," in *Anais do I Congresso UniSENAI-SP de Educação, Tecnologia e Inovação*, 2024, DOI: 10.29327/congressosenai-sp.

[24] P. Rojnarong and W. Pora, "Signal Strength and Energy Consumption on Various Internet of Things Communication Protocol Using Heltec ESP32 LoRa," in *2024 21st International Joint Conference on Computer Science and Software Engineering (JCSSE)*, pp. 626–630, 2024, DOI: 10.1109/JCSSE61278.2024.10613704.

[25] E. Damasso and L. Correia, "COST 231 Final Report: Digital Mobile Radio Towards Future Generation Systems," *European Commission, Directorate General XIII, Report No. RJR*, vol. 18957, p. 516, 1999.

[26] L. Schirru, M. B. Lodi, A. Fanti, and G. Mazzarella, "Improved COST 231-WI Model for Irregular Built-Up Areas," in *2020 XXXIIIrd General Assembly and Scientific Symposium of the International Union of Radio Science*, pp. 1–4, 2020, DOI: 10.23919/URSIGASS49373.2020.9232010.

[27] S. Corporation, "SX1276/77/78/79 - LoRa Modem Designers Guide," pp. 1–133, 2016.

[28] Semtech, "SX1301 Datasheet," pp. 1–41, 2016.

[29] F. S. Sousa, I. R. S. Casella, and C. E. Capovilla, "Efeitos da Colisão e Interferência em Redes Ultra-Densas LoRaWAN," in *2021 14th IEEE International Conference on Industry Applications (INDUSCON)*, pp. 524–530, 2021, DOI: 10.1109/INDUSCON51756.2021.9529631.

[30] C. Goursaud and J.-M. Gorce, "Dedicated Networks for IoT: PHY/MAC State of the Art and Challenges," *EAI Endorsed Transactions on Internet of Things*, vol. 1, no. 1, p. e3, 2015, DOI: 10.4108/eai.26-10-2015.150597.

[31] O. Afisiadis, A. Burg, and A. Balatsoukas-Stimming, "Coded LoRa Frame Error Rate Analysis," in *ICC 2020 - 2020 IEEE International Conference on Communications (ICC)*, pp. 1–6, 2020, DOI: 10.1109/ICC40277.2020.9148806.

[32] T. Elshabrawy and J. Robert, "Closed-Form Approximation of LoRa Modulation BER Performance," *IEEE Communications Letters*, vol. 22, no. 9, pp. 1778–1781, 2018, DOI: 10.1109/LCOMM.2018.2849718.

[33] D. Zorbas, K. Abdelfadeel, P. Kotzanikolaou, and D. Pesch, "TS-LoRa: Time-slotted LoRaWAN for the Industrial Internet of Things," *Computer Communications*, vol. 153, pp. 1–10, 2020, DOI: 10.1016/j.comcom.2020.01.056.

[34] D. Kjendal, "LoRa-Alliance Regional Parameters Overview," *Journal of ICT Standardization*, vol. 9, no. 1, pp. 35–46, 2021, DOI: 10.13052/jicts2245-800X.914.

[35] F. S. Sousa, I. R. S. Casella, and C. E. Capovilla, "Uplink Performance of Massive LoRaWAN," in *2023 SBMO/IEEE MTT-S International Microwave and Optoelectronics Conference (IMOC)*, pp. 22–24, 2023, DOI: 10.1109/IMOC57131.2023.10379741.

[36] L. Casals, B. Mir, R. Vidal, and C. Gomez, "Modeling the Energy Performance of LoRaWAN," *Sensors*, vol. 17, no. 10, 2017, DOI: 10.3390/s17102364.

[37] Y. H. Tehrani, A. Amini, and S. M. Atarodi, "A Tree-Structured LoRa Network for Energy Efficiency," *IEEE Internet of Things Journal*, vol. 8, no. 7, pp. 6002–6011, 2021, DOI: 10.1109/JIOT.2020.3034142.

[38] D. Deng, "Li-ion Batteries: Basics, Progress, and Challenges," *Energy Science & Engineering*, vol. 3, no. 5, pp. 385–418, 2015, DOI: 10.1002/ese3.95.

[39] A. Waret, M. Kaneko, A. Guitton, and N. E. Rachkidy, "LoRa Throughput Analysis with Imperfect Spreading Factor Orthogonality," *CoRR*, vol. abs/1803.06534, 2018, DOI: 10.48550/arXiv.1803.06534.